applied optics

Optical function of the finite-thickness corrugated pellicle of euglenoids

MARINA E. INCHAUSSANDAGUE,[1,2,*] DIANA C. SKIGIN,[1,2] AND ANDRÉS E. DOLINKO[3,4]

[1]Universidad de Buenos Aires, Facultad de Ciencias Exactas y Naturales, Departamento de Física, Grupo de Electromagnetismo Aplicado, Buenos Aires, Argentina
[2]CONICET—Universidad de Buenos Aires, Instituto de Física de Buenos Aires (IFIBA), Buenos Aires, Argentina
[3]Universidad de Buenos Aires, Facultad de Ciencias Exactas y Naturales, Departamento de Biodiversidad y Biología Experimental, Laboratorio de Micología, Buenos Aires, Argentina
[4]CONICET—Universidad de Buenos Aires, Instituto de Micología y Botánica (INMIBO), Buenos Aires, Argentina
*Corresponding author: mei@df.uba.ar

Received 7 April 2017; revised 16 May 2017; accepted 19 May 2017; posted 22 May 2017 (Doc. ID 292375); published 12 June 2017

We explore the electromagnetic response of the pellicle of selected species of euglenoids. These microorganisms are bounded by a typical surface pellicle formed by S-shaped overlapping bands that resemble a corrugated film. We investigate the role played by this structure in the protection of the cell against UV radiation. By considering the pellicle as a periodically corrugated film of finite thickness, we applied the C-method to compute the reflectance spectra. The far-field results revealed reflectance peaks with a Q-factor larger than 10^3 in the UV region for all the illumination conditions investigated. The resonant behavior responsible for this enhancement has also been illustrated by near-field computations performed by a photonic simulation method. These results confirm that the corrugated pellicle of euglenoids shields the cell from harmful UV radiation and open up new possibilities for the design of highly UV-reflective surfaces.

OCIS codes: (310.0310) Thin films; (310.6860) Thin films, optical properties; (350.2770) Gratings.

https://doi.org/10.1364/AO.56.005112

1. INTRODUCTION

Evolutionary processes in living organisms have developed a remarkable variety of intricate and detailed structures that exhibit singular electromagnetic properties. Depending on the optical mechanisms involved, the interaction of light with these complex microstructures produces different effects, such as iridescent colors, metallic appearance, and extremely pure colors [1–5]. It is not only visual effects that can be generated; depending on the typical size of the geometrical parameters of the structure, interesting features can be found in regions of the spectrum other than the visible, such as the ultraviolet (UV) and the infrared. These features might be employed by the owner species for thermal regulation and UV protection. For instance, the high-altitude flower *Leontopodium alpinum* (Edelweiss) has a UV protection mechanism based on the use of guided modes along fibers containing UV-absorbing material, which have nanometric photonic structures acting as wavelength-selective couplers [6,7]. The jumping spider *Cosmophasis umbratica* produces a UV reflection peak that is very important in mating displays [8], and also UV-reflecting decorations in spider webs have been reported to act as a visual display that attracts prey [9].

Euglenoids are a group of predominantly free-living unicellular flagellates that mostly live in freshwater bodies but can also be found in marine and brackish waters. These organisms show a typical surface structure that distinguishes them from the other flagellates: most cells are bounded by a pellicular complex formed by overlapping bands (strips), which have a stable maximum number for each species and can be arranged either longitudinally or helicoidally. It is well known that euglenoids have developed numerous protection mechanisms intended to avoid or reduce the damage produced by UV radiation. The most studied ones are of chemical origin, such as the production of pigments and the repair mechanisms in hours of darkness as well as during daylight [10–13].

In a previous work, we determined the cell viability of three species of euglenoids after a UV radiation treatment. Basically, this study showed that the species *Euglena gracilis* and *Peranema trichophorum*, which have a regularly corrugated pellicle, mostly survive UV radiation, whereas *Monomorphyna megalopsis*, whose pellicle exhibits large planar regions (in comparison to the UV wavelengths), does not [14]. Prompted by this result, we also explored the possible protection that could provide the surface pellicle against UV radiation from an electromagnetic point of view, by modeling the cell surface as a periodic interface of various shapes between two semi-infinite media [14,15], and also by considering the whole cell as an infinite cylinder

with a transverse cross section that resembles the euglenoid's profile [16]. Previous results suggest that the periodically patterned interface could potentially contribute to the UV protection of the cell, and that the pellicle characteristics (depth, period, shape) are critical parameters that strongly affect the electromagnetic response. It is important to remark that in these studies the thickness of the pellicle was neglected, and only the effect of its corrugations was evaluated. However, it has been reported that models representing the microalga as a coated sphere, where the coating represents the cell wall, can better reproduce its scattering properties than a bare homogeneous sphere [17].

To gain further insight into the influence of the corrugated pellicle on the electromagnetic performance, in this paper we refine our model and consider the pellicle as a periodically corrugated film of finite thickness. We apply the C-method [18–22] to calculate the reflected response of the structure for different angles of incidence (in classical as well as in conical mounting) and for different polarization modes. We also investigate the near field in the vicinity of the structure. To perform this calculation, we employ a photonic simulation method (PSM) especially suitable for dealing with complex biological structures [23].

The organization of the paper is as follows. The characteristics of the structure under study are shown in Section 2. These features are employed in Section 3 to establish the geometrical model employed for the calculations. In this section we also outline the electromagnetic methods employed to solve the diffraction problem: the C-method and the PSM. The results obtained are shown in Section 4, where we include far-field computations of reflectance for different incidence angles and polarization modes, as well as near-field maps for resonant and nonresonant wavelengths. Finally, concluding remarks are given in Section 5.

2. STRUCTURE CHARACTERIZATION

Figure 1 shows transmission electron microscopy (TEM) images of *E. gracilis* and *P. trichophorum* cells, and detailed images of their pellicles. These images were taken by a ZEISS EM 10 electron microscope available in the Electron Microscopy Service of the Facultad de Ciencias Exactas y Naturales, Universidad de Buenos Aires. It can be observed that the profile of the pellicles exhibits a quite regular pattern that resembles a corrugated film. However, as expected for natural structures, the distance between adjacent grooves varies from one individual to another, and even in different regions within the same pellicle. According to measurements done in images of several individuals of *E. gracilis* and *P. trichophorum*, the reported periods range between 0.1 and 0.6 μm, their depths vary between 0.04 and 0.4 μm [15], and their thicknesses between 0.004 and 0.9 μm.

For the case of *E. gracilis*, the refractive indices of the components of the pellicle complex and the plasmatic membrane range between 1.46 and 1.6 [24]. These values correspond to the visible range; measurements of the refractive indices in the UV region are not found in the literature. Since the pellicle is a highly conserved character in euglenoids, it can be assumed that the pellicles of other species such as *P. trichophorum* have a similar composition. On the other hand, the refractive indices of the intracellular organelles constituting the eukaryotic microalgae (nucleus, mitochondria, cytoplasm, chloroplast) range between 1.36 and 1.6 [17,25–29].

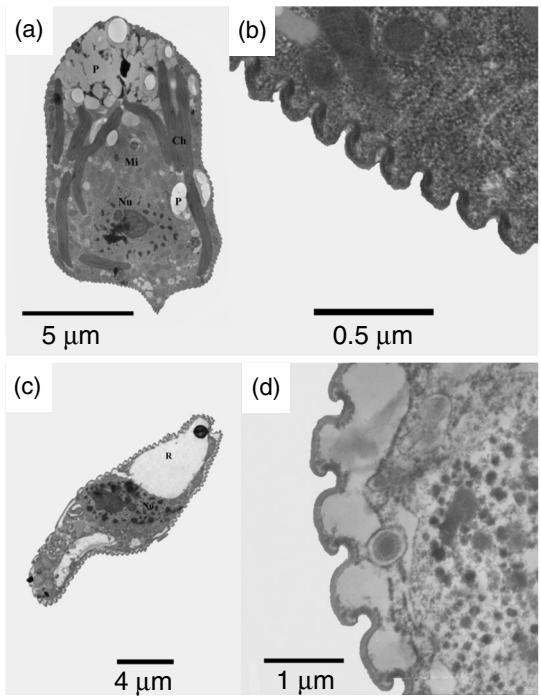

Fig. 1. TEM images of the species under study. (A) *Euglena gracilis* cell and (B) detailed image of its pellicle, (C) *Peranema trichophorum* cell and (D) detailed image of its pellicle. P, paramylon; Nu, nucleus; Ch, chloroplast; Mi, mitochondria; R, reservoir. The scale bars are indicated in each figure.

3. CONFIGURATION AND METHODS

Since we are interested in exploring the specific role of the finite thickness of the pellicle and that of the periodic pattern in the protection mechanism, we assume that the pellicle is a perfectly periodic corrugated thin film of finite thickness that separates the external medium from the interior of the cell (see Fig. 2).

A. C-method

The geometry of the problem is shown in Fig. 2. The regions $y > y_2(x)$, $y_1(x) < y < y_2(x)$, and $y < y_1(x)$ are filled by

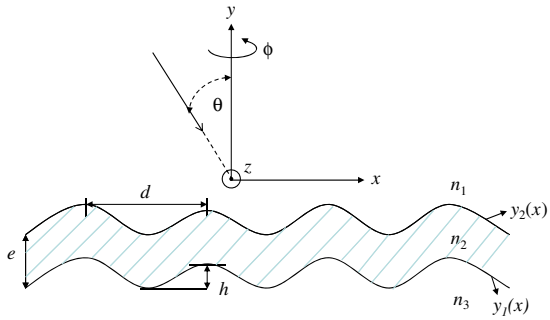

Fig. 2. Geometry of the diffraction problem.

homogeneous and lossless dielectric materials with refractive indices n_1, n_2, and n_3, respectively. The grooves of the grating are along the z axis, and the y axis is perpendicular to the mean surface of the grating. A linearly polarized electromagnetic plane wave is incident from medium 1 at an angle θ with respect to the y axis; ϕ is the angle between the xy plane and the plane of incidence. The angular frequency is $\omega = ck = c2\pi/\lambda$, where c is the velocity of light in vacuum and λ is the wavelength in vacuum. The grating surface $y = y_1(x)$ is periodic such that $y_1(x \pm d) = y_1(x)$ with d as the period, and the coating thickness e is uniform so that $y_2(x) = y_1(x) + e$.

To solve the electromagnetic problem, we used a computer code based on the C-method, the details of which are available elsewhere [18–22]. The main idea of the C-method is to simplify the boundary conditions by using a nonorthogonal curvilinear coordinate transformation that maps the grating interfaces onto planes. The numerical code yields the efficiencies of the reflected and transmitted diffraction orders, wherefrom the total reflectance and total transmittance for TE and TM polarizations are obtained. Although our computational method is suitable for grooves of arbitrary shape, for the purpose of this paper we chose to restrict our attention to sinusoidal gratings with groove depth h.

B. Photonic Simulation Method

The PSM simulates the propagation of electromagnetic waves via an analogy with the propagation of transverse mechanical waves in a planar network of particles coupled by elastic springs [23,30]. The movement of the particles is constrained to the transverse direction (z), i.e., to the direction normal to the plane of the two-dimensional array, the (x, y) plane. A wave is generated by applying a transverse external force to certain particles. For a highly dense array, the system can be regarded as a continuous medium representing a tensioned elastic membrane with mass density $\mu(x, y)$. The time evolution of the system is described by the following wave equation:

$$\frac{\partial^2 A}{\partial t^2} = \frac{T}{\mu}\nabla^2 A - \frac{\gamma}{\mu}\frac{\partial A}{\partial t} + \frac{E_t}{\mu}, \tag{1}$$

where $A = A(x, y, t)$ is the position along the z axis of a differential element of the membrane, T is the tension of the membrane, $\gamma = \gamma(x, y)$ is a damping constant, and $E_t = E_t(x, y)$ is the time-varying applied external force. $v = \sqrt{T/\mu}$ represents the speed of the waves. In analogy with optics, regions with mass density μ_0 can be identified with vacuum, i.e., a medium of refractive index $n_0 = 1$, whereas a region with an arbitrary mass density μ corresponds to a medium with a real part of the refractive index $n = \sqrt{\mu/\mu_0}$. This approach can be applied to two-dimensional problems involving dielectric materials illuminated by TE-polarized light. Further details can be found in [23,30].

4. RESULTS

In order to elucidate whether the pellicle of the cell plays a protective role against UV radiation, in this section we explore its electromagnetic response along the UV and visible ranges. In the examples below we illustrate the behavior of such a structure for typical parameters (depth-to-period ratio, refractive indices) found in the studied species of euglenoids, and analyze the response for different incidence angles and polarization modes. We first investigate the far-field response of the structure, and then we compute the near field for resonant and nonresonant situations.

A. Far Field

A perfectly periodic corrugated thin film constitutes a simplified model to investigate the electromagnetic response of the euglenoid's pellicle. In particular, the reflectance of the structure in the UV and visible ranges provides information about a potential protection mechanism of structural origin provided by the cell's pellicle.

Since euglenoids are aquatic organisms, the refractive index of the incidence medium (n_1) is set to be 1.35, which corresponds to the average refractive index of water in the near-UV range [31]. Regarding the refractive index of the interior of the cell, several recent works have been devoted to improving the modeling of eukaryotic microalgae in order to accurately predict their electromagnetic response [17,26–29]. One of the proposed models consists of a homogeneous sphere characterized by an effective refractive index calculated from the optical properties of the different organelles [17,26,28,29]. In these works, the authors also present an improved model of a coated sphere with a coating corresponding to the cell wall and a homogeneous core with a volume-averaged refractive index. The effect of the cell wall on the scattering coefficient was also studied in Ref. [27]. Taking into account the reported values of the refractive indices of the cell wall and core, we assumed for the pellicle $n_2 = 1.5$, and for medium 3, which corresponds to the cell core, we used $n_3 = 1.38$ and 1.4 to consider possible variations within the UV range.

In Fig. 3 we plot the total reflectance (R) spectra of a periodic corrugated film like that shown in Fig. 2, with $h/d = 1.27$, $e/d = 0.3$, $n_1 = 1.35$, and $n_2 = 1.5$, illuminated in classical mounting (the incidence plane, which includes the incident wave vector and the y axis, coincides with the main section of the structure), i.e., $\phi = 0$ (see Fig. 2). Figures 3(a) and 3(b) correspond to $n_3 = 1.38$, whereas Figs. 3(c) and 3(d) correspond to $n_3 = 1.4$. We consider different incidence angles θ and both polarization modes: TE [Figs. 3(a) and 3(c)] and TM [Figs. 3(b) and 3(d)]. The range of λ/d was chosen to include the UV region for typical values of the pellicle's period. It is observed that in all cases the reflected response is characterized by a set of peaks with very high reflectance, distributed all along the range of wavelengths considered. By defining the quality factor as $Q = \lambda_{\text{res}}/\Delta\lambda$, with λ_{res} being the peak wavelength and $\Delta\lambda$ the total width at half-maximum, the Q-factors of the main peaks in Fig. 3 take values larger than 10^3. These peaks correspond to Fano resonances that originate at the film surface. Fano resonances are characterized by an asymmetric line profile, and this asymmetry originates from the close coexistence of resonant transmission and resonant reflection and can be reduced to the interaction of a discrete (localized) state with a continuum of propagation modes [32,33]. The peaks shown in Fig. 3 are similar to those found in [6], and, as expected, their intensity varies with the incidence angle and polarization mode.

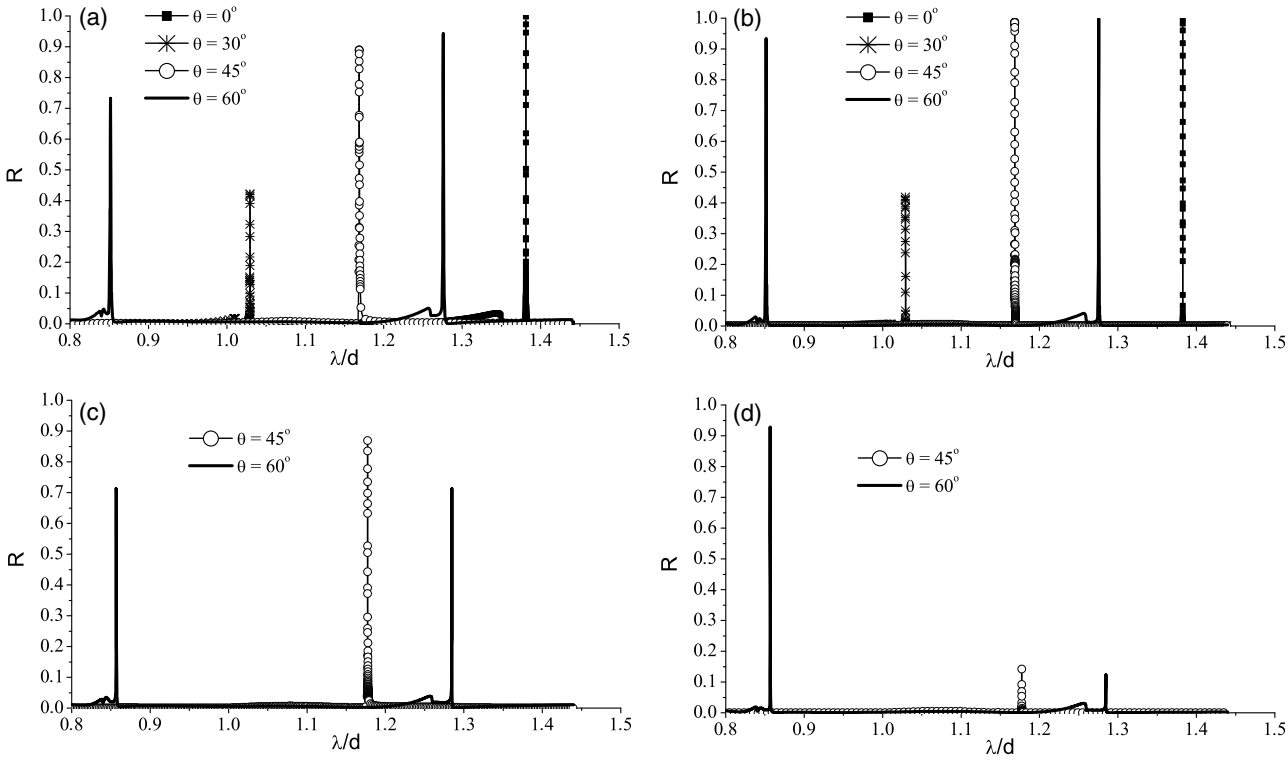

Fig. 3. Reflectance of a periodic corrugated film with $h/d = 1.27$, $e/d = 0.3$, $n_1 = 1.35$, and $n_2 = 1.5$, illuminated at classical mounting, for several values of θ. (a) $n_3 = 1.38$, TE polarization, (b) $n_3 = 1.38$, TM polarization, (c) $n_3 = 1.4$, TE polarization, (d) $n_3 = 1.4$, TM polarization.

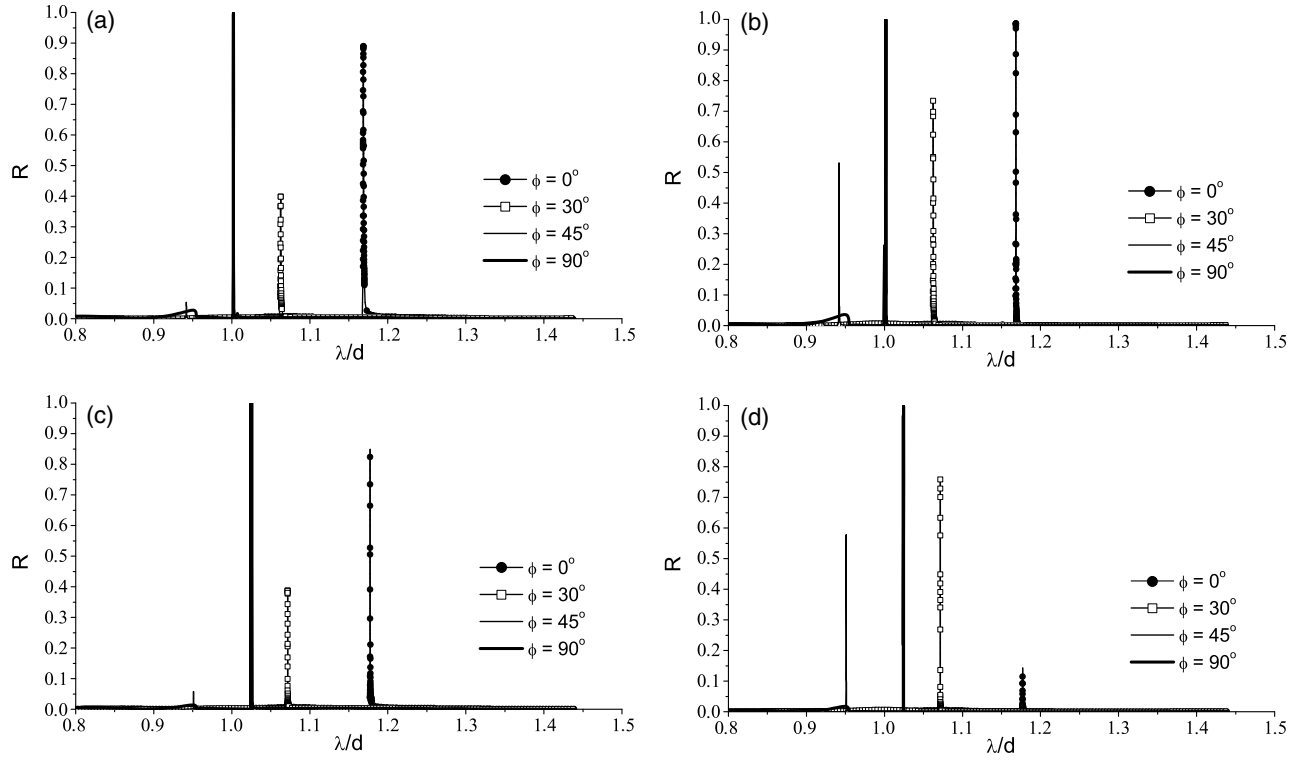

Fig. 4. Reflectance of a periodic corrugated film with $h/d = 1.27$, $e/d = 0.3$, $n_1 = 1.35$, and $n_2 = 1.5$, illuminated at conical mounting, with $\theta = 45°$ and for several values of ϕ. (a) $n_3 = 1.38$, TE polarization, (b) $n_3 = 1.38$, TM polarization, (c) $n_3 = 1.4$, TE polarization, (d) $n_3 = 1.4$, TM polarization.

Similar behavior is found when conical mounting illumination conditions are considered, i.e., when the incidence plane forms an angle ϕ with the main section of the structure, as shown in Fig. 4 for both polarization modes. The existence of such peaks reveals a resonant coupling between the incident radiation and the modes supported by the finite-thickness corrugated film. More specifically, these peaks are spectrally located near the Rayleigh anomalies (RAs) [34], i.e., the wavelengths at which a grazing diffraction order propagates along the structure. The RA wavelengths are obtained by imposing a grazing p diffraction order ($\theta_p = 90°$) in the grating equation obtained via application of the pseudoperiodicity condition on the tangential electromagnetic fields. In the case of conical mounting, this condition takes the form

$$\cos\phi = \frac{\omega n_1 \cos^2\theta d}{4\pi c p \sin\theta} - \frac{p\pi c}{d\omega n_1 \sin\theta} + \frac{\omega d(n_3^2 - n_1^2)}{4\pi p n_1 \sin\theta} \quad \textbf{(2)}$$

for the transmitted diffraction orders, and for the reflected ones the same relationship holds, but without the third term. In Eq. (2), c is the velocity of light in vacuum. In addition, if $n_1 = n_3$, the third term in Eq. (2) vanishes, and then the conditions for grazing reflected and transmitted orders become identical. Equation (2) gives the pairs of incidence angles (θ, ϕ) for which the p diffraction order propagates along the surface given n_1, n_3, and ω.

In Figs. 5 and 6 we plot Eq. (2) for the grazing transmitted and reflected diffraction orders. Figure 5 shows the trajectories of the grazing orders in the ($\theta - \lambda/d$) plane for fixed values of ϕ: 0° [classical mounting, Fig. 5(a)], 30° [Fig. 5(b)], 45° [Fig. 5(c)], and 60° [Fig. 5(d)]. In Fig. 6 we consider four values of θ and plot the trajectories in the ($\phi - \lambda/d$) plane. The solid lines correspond to reflected orders, and the dotted lines to transmitted orders. The label near each curve indicates the p grazing order and its type, reflected (R) or transmitted (T). Notice that the paths of the reflected and the transmitted orders are slightly different because the incident and the transmission media have refractive indices that differ only by 0.03. It is important to note that the trajectories shown in Figs. 5 and 6 are independent of the polarization mode, meaning that the RAs' wavelengths coincide for both TE and TM polarizations. These figures help correlate the spectral locations of the resonant peaks with the surface modes of the grating. For instance, Fig. 5(a) can be compared with Fig. 3. Each horizontal dashed line indicated in Fig. 5(a) corresponds to a particular value of θ.

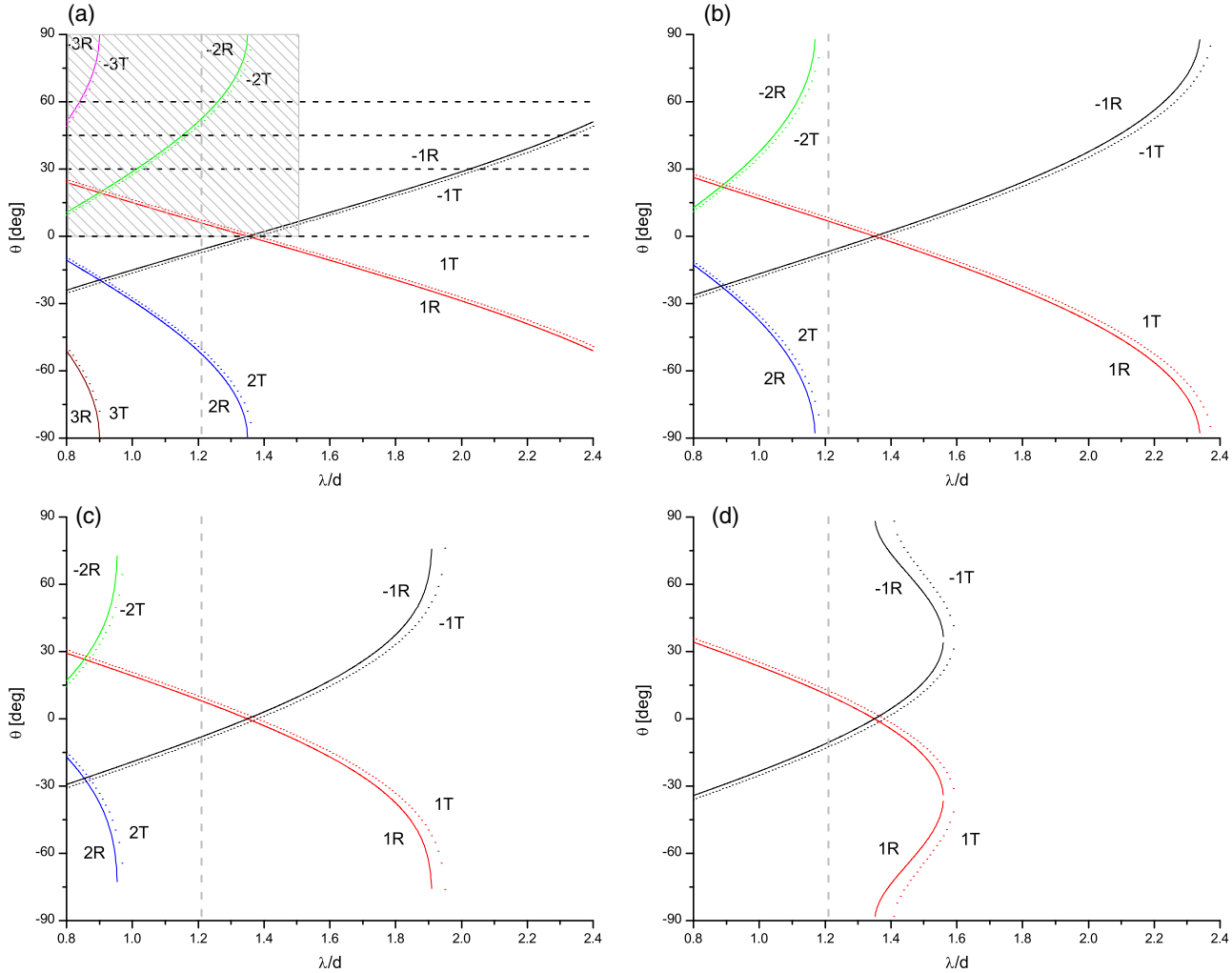

Fig. 5. Trajectories of the Rayleigh anomalies in the $\theta - \lambda/d$ plane for several values of ϕ: (a) 0°, (b) 30°, (c) 45°, and (d) 60°. The shaded zone in (a) corresponds to the amplified region shown in Fig. 7(b).

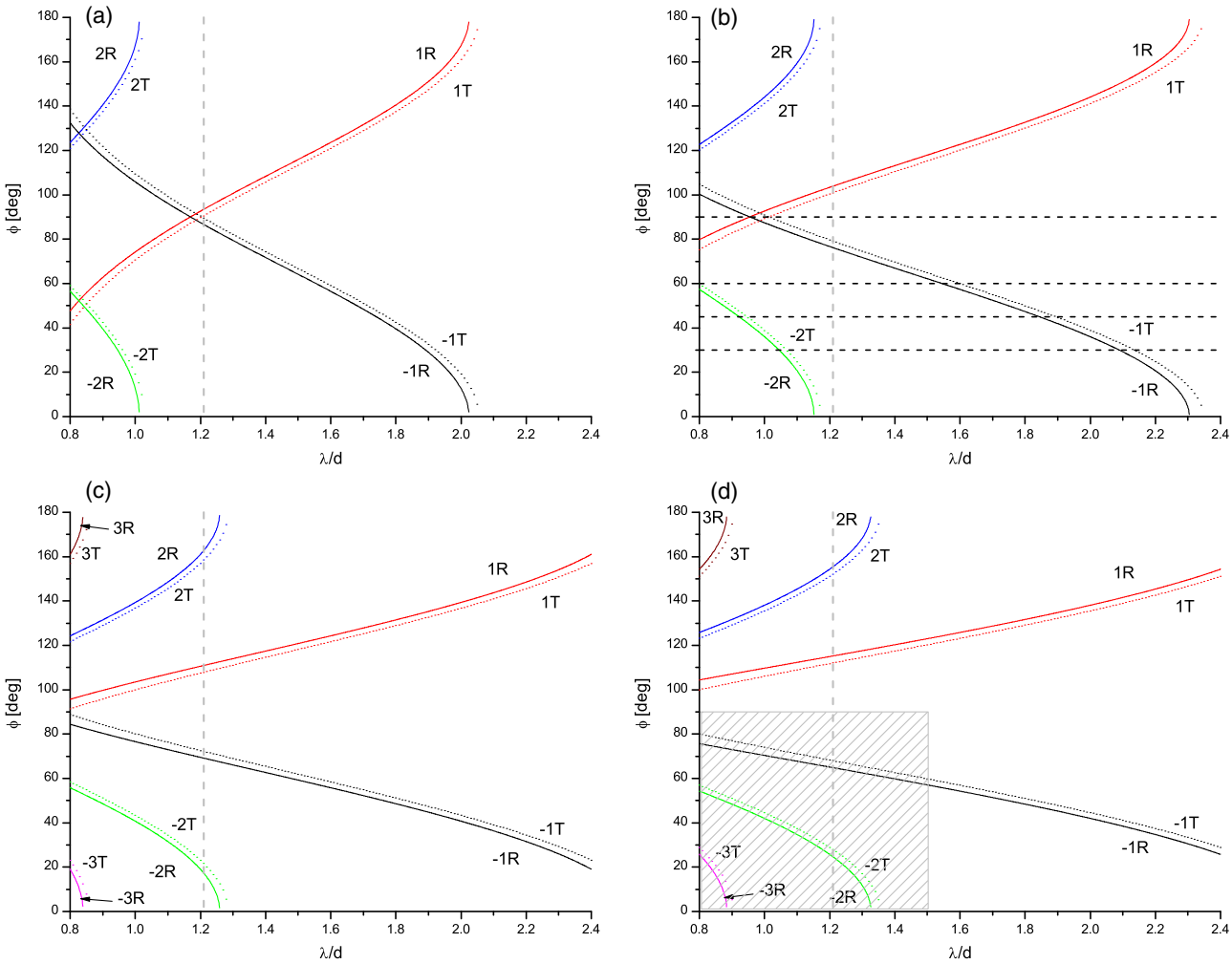

Fig. 6. Trajectories of the Rayleigh anomalies in the $\phi - \lambda$ plane for several values of θ: (a) 30°, (b) 45°, (c) 60°, and (d) 75°. The shaded zone in (d) corresponds to the amplified region shown in Fig. 7(d).

For example, the lowest dashed line at $\theta = 0$ can be related with the black squares curves in Figs. 3(a) and 3(b). A clear correspondence between the spectral locations of the peaks and the RA condition is observed. The maxima in Fig. 3 that exhibit a double peak, for instance, for $\theta = 60°$, can be associated with both the reflected and the transmitted RAs for the same order. This behavior is also found for $\phi \neq 0$, i.e., under conical mounting illumination, as observed in Fig. 6(b) ($\theta = 45°$), which can be compared with Figs. 4(a) and 4(b). The horizontal dashed lines in Fig. 6(b) indicate the values of ϕ considered in Fig. 4. The vertical dashed lines in Figs. 5 and 6 at $\lambda/d \approx 1.2$ provide a reference for the spectral limit between the UV and the visible ranges ($\lambda = 380$ nm) for $d = 314$ nm, which is a typical value of the period found in the euglenoids' pellicle. However, since the measured values of the period range between 100 and 600 nm, the UV limit could reach $\lambda/d = 2.4$. Taking into account all four panels in Figs. 5 and 6, it is observed that there is a higher concentration of RAs for shorter wavelengths, which, in turn, produce more resonant reflectance peaks within this spectral region.

It is evident that the reflectance peaks originate from resonant coupling between the grazing diffraction orders and the eigenmodes of the grating. In order to get more insight into the role played by each type of diffraction order (R or T) in the generation of the reflectance peaks, in Fig. 7 we show color maps of total reflectance R for the cases illustrated in Figs. 5(a) and 6(d) for TE polarization. In Fig. 7(a) we consider $\phi = 0°$ and vary θ and λ/d, and in Fig. 7(c) $\theta = 75°$, and ϕ and λ/d are varied. For these maps, we scan the variables over a reduced region indicated by a shaded zone in Figs. 5(a) and 6(d), respectively. For clarity, the corresponding plots of RAs are shown in Figs. 7(b) and 7(d).

The correlation between the spectral locations of the reflectance peaks and the corresponding RAs is evident. It is observed that the highest-quality peaks [thin lines in Figs. 7(a) and 7(c)] correspond to the grazing transmitted orders, indicated by dotted lines in Figs. 7(b) and 7(d). However, the grazing reflected orders give rise to secondary, lower-quality peaks with Q-factors of the order of 50 (wider bands with much lower intensity next to the fine peaks), as also observed in Figs. 3 and 4 for large values of θ.

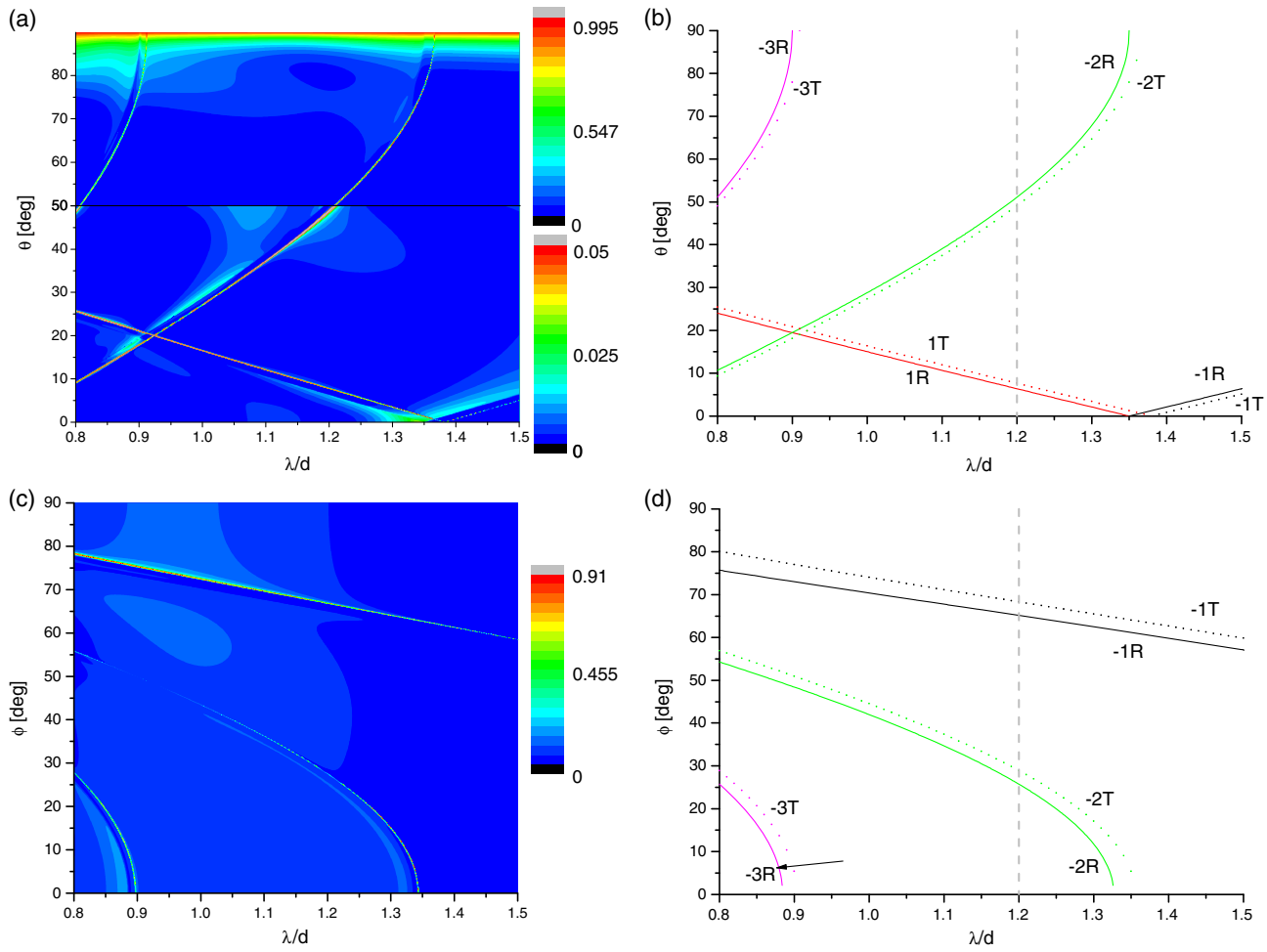

Fig. 7. Comparison between the total reflected efficiency and the spectral location of Rayleigh anomalies for a grating with $h/d = 1.27$, $e/d = 0.3$, $n_1 = 1.35$, $n_2 = 1.5$, and $n_3 = 1.38$. (a) Color map of total reflected efficiency as a function of λ/d and θ for $\phi = 0°$ and TE polarization. Notice that the lower ($\theta < 50°$) and the upper ($\theta > 50°$) parts of this figure have different color scales; in the lower region the color scale is saturated at a maximum of 0.05 (red) to better visualize the features of the plot. (b) Trajectories of the Rayleigh anomalies in the $\theta - \lambda/d$ plane for $\phi = 0°$, (c) color map of total reflected efficiency as a function of λ/d and ϕ for $\theta = 75°$ and TE polarization, (d) trajectories of the Rayleigh anomalies in the $\phi - \lambda/d$ plane for $\theta = 75°$.

B. Near Field

It is also interesting to compare the near-field distributions in and out of resonance. For this purpose, we employed the PSM to compute the electric field in the vicinity of the grating for $\theta = \phi = 0$. Taking into account that the PSM is an essentially numerical method, the simulation domain and the width of the incident beam should be finite. For this calculation we consider a rectangular domain of $31.8d \times 10d$ (d is the grating period), and the incident field is a Gaussian beam of width $\sigma = 5.1d$. The rest of the parameters are the same as those used in the previous figures: $h/d = 1.27$, $e/d = 0.3$, $n_1 = 1.35$, $n_2 = 1.5$, and $n_3 = 1.38$. In Fig. 8 we plot $|\vec{E}|^2$ for a resonant case [Fig. 8(a)] and for a nonresonant case [Fig. 8(b)]. Both plots are normalized to the maximum value of $|\vec{E}|^2$ in Fig. 8(a), so that the color scale is the same for both panels. The incident beam comes from the top. In both cases the near field exhibits intensification spots in the vicinity of the corrugated slab. However, notice that in the resonant case these spots are found at both sides of the film, i.e., at the incident and at the transmission side of the film. The intensification at the incident medium gives rise to an enhancement of the reflectance, as observed in Figs. 3, 4, and 7. On the other hand, in the nonresonant case the hot spots are only found in the transmission medium. It is important to note that the PSM and the C-method are complementary approaches, used here to address different aspects of the same problem. Consequently, due to the finite nature of the simulation domain in the PSM, the near-field maps in Fig. 8 do not correspond, strictly speaking, to the perfectly periodic system explored in the previous subsection. Nevertheless, they serve as a qualitative confirmation of the resonant behavior in corrugated films.

5. DISCUSSION AND CONCLUSIONS

We have investigated, from an electromagnetic point of view, the role played by the euglenoid's pellicle in the protection

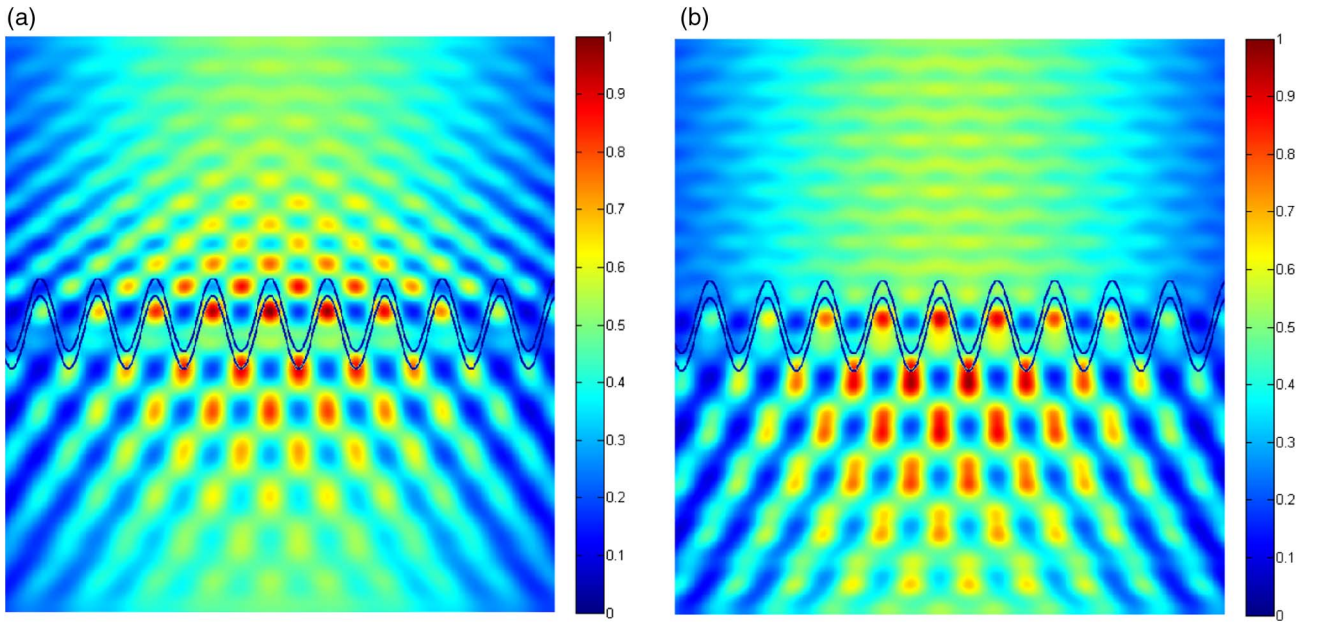

Fig. 8. Normalized near-field distribution (a) at resonance and (b) out of resonance. The grating and illumination parameters are $h/d = 1.27$, $e/d = 0.3$, $n_1 = 1.35$, $n_2 = 1.5$, $n_3 = 1.38$, $\theta = \phi = 0°$, and $\sigma = 5.1d$.

against UV radiation. We have modeled the pellicle as a corrugated sinusoidal film of finite thickness and applied the C-method to compute the reflectance spectra. To calculate the electromagnetic response, it is necessary to introduce the geometrical parameters of the pellicle (height, thickness, period), the refractive indices of the media involved, and the incidence conditions (angle of incidence, polarization). The values of h/d and e/d used for the simulations have been obtained from TEM images of *E. gracilis* and *P. trichophorum*. The refractive indices of the different parts of the cell in the UV range have been extrapolated from published data available in the visible range. In their natural habitat euglenoids are exposed to sunlight, and therefore they are illuminated under all incidence angles and both polarization modes. Taking into account the fact that the electromagnetic behavior of the cell can be computed as a continuous superposition of the individual responses for each pair of angles of incidence (θ, ϕ), we have chosen a few representative angles to calculate the reflectance as a function of the wavelength. The far-field results revealed very high Q reflectance peaks in the UV region for all the illumination conditions investigated. These curves suggest that the excitation of resonances within the corrugated pellicle increases the reflectance. Therefore, this mechanism could contribute to reducing the penetration of UV radiation into the interior of the cell, thus minimizing the damage and increasing the survival of these organisms. This resonant behavior has also been illustrated by near-field computations.

The above results suggest that the first barriers of the euglenoid's cell could play an important role in the protection against UV radiation. The optical features found can be useful for diverse technological applications. For instance, based on structural mechanisms, biomimetic artificial structures are being designed and developed that can produce a predesigned effect [35], such as different kinds of fabrics that are being explored to provide protection against UV radiation [36].

However, there are still several aspects that should be investigated. It is known that some species of euglenoids possess pigments in their composition. Therefore, it would be worth exploring the role of pigments in the electromagnetic response of the cell. In the case of nonpigmented euglenoids such as *P. trichophorum*, an increase in the reflectance necessarily implies a reduction in the transmittance. It would also be interesting to know if the pigments present in *E. gracilis* also contribute to its protection against UV radiation. In this case, the absorptance of the cell could be an additional indicator of this kind of protective mechanism.

The simplified model of a perfectly periodic corrugated film used in this work assumes an effective refractive index for the interior of the cell. Another interesting aspect to be considered would be the variability of the refractive indices from point to point of the cell. The PSM employed here for the computation of the near field could eventually account for these inhomogeneities and also for the imperfections of the film profile, thus providing a more accurate representation of the sample. However, it should be mentioned that far-field calculations employing the PSM are highly computationally demanding.

Taking into account that these kinds of structures could inspire the design of highly UV-reflective surfaces, it would also be interesting to explore how the electromagnetic response is affected by the geometry of the structure, in order to optimize the profiles for maximum UV reflectance.

Funding. Consejo Nacional de Investigaciones Científicas y Técnicas (CONICET) (PIP 112-201101-00451); Universidad de Buenos Aires (UBA) (UBACyT 20020150100028BA).

REFERENCES

1. A. Parker, "515 million years of structural colour," J. Opt. A **2**, R15–R28 (2000).
2. M. Srinivasarao, "Nano-optics in the biological world: beetles, butterflies, birds, and moths," Chem. Rev. **99**, 1935–1962 (1999).
3. P. Vukusic and J. R. Sambles, "Photonic structures in biology," Nature **424**, 852–855 (2003).
4. S. Kinoshita, *Structural Colors in the Realm of Nature* (World Scientific, 2008).
5. S. Berthier, *Iridescences, the Physical Colours of Insects* (Springer, 2007).
6. J.-P. Vigneron, M. Rassart, Z. Vértesy, K. Kertész, M. Sarrazin, L. P. Biro, D. Ertz, and V. Lousse, "Optical structure and function of the white filamentary hair covering the edelweiss bracts," Phys. Rev. E **71**, 011906 (2005).
7. K. Kertész, Z. Bálint, Z. Vértesy, G. I. Márk, V. Lousse, J.-P. Vigneron, and L. P. Biro, "Photonic crystal type structures of biological origin: structural and spectral characterization," Curr. Appl. Phys. **6**, 252–258 (2006).
8. M. F. Land, J. Horwood, M. L. M. Lim, and D. Li, "Optics of the ultraviolet reflecting scales of a jumping spider," Proc. R. Soc. B **274**, 1583–1589 (2007).
9. C. L. Craig and G. D. Bernard, "Insect attraction to ultraviolet-reflecting spider webs and web decorations," Ecology **71**, 616–623 (1990).
10. P. L. Jokiel and R. H. York, Jr., "Importance of ultraviolet radiation in photoinhibition of microalgal growth," Limnol. Oceanogr. **29**, 192–198 (1984).
11. L. Franklin and R. Forster, "The changing irradiance environment: consequences for marine macrophyte physiology, productivity and ecology," Eur. J. Phycol. **32**, 207–232 (1997).
12. G. A. Ekelund, "Interactions between photosynthesis and 'light-enhanced dark respiration' (LEDR) in the flagellate Euglena gracilis after irradiation with ultraviolet radiation," J. Photochem. Photobiol. B **55**, 63–69 (2000).
13. D. Karentz, F. S. McEuen, M. C. Land, and W. C. Dunlap, "Survey of mycosporine-like amino acid compounds in Antarctic marine organisms: potential protection from ultraviolet exposure," Marine Biol. **108**, 157–166 (1991).
14. M. E. Inchaussandague, D. C. Skigin, A. Tolivia, I. Fuertes Vila, and V. Conforti, "Electromagnetic response of the protective pellicle of different unicellular microalgae," Proc. SPIE **9055**, 905514 (2014).
15. M. E. Inchaussandague, M. L. Gigli, D. C. Skigin, A. Tolivia, and V. Conforti, "Electromagnetic response of the protective pellicle of Euglenoids: influence of the surface profile," Proc. SPIE **9429**, 94290D (2015).
16. A. Dolinko, C. Valencia, D. C. Skigin, M. E. Inchaussandague, A. Tolivia, and V. Conforti, "UV protection of euglenoids: computation of the electromagnetic response," Proc. SPIE **9531**, 953144 (2015).
17. A. Bhowmik and L. Pilon, "Can spherical eukaryotic microalgae cells be treated as optically homogeneous?" J. Opt. Soc. Am. A **33**, 1495–1503 (2016).
18. J. Chandezon, M. Dupuis, G. Cornet, and D. Maystre, "Multicoated gratings: a differential formalism applicable in the entire optical region," J. Opt. Soc. Am. **72**, 839–846 (1982).
19. L. Li, "Oblique-coordinate-system-based Chandezon method for modeling one-dimensionally periodic, multilayer, inhomogeneous, anisotropic gratings," J. Opt. Soc. Am. A **16**, 2521–2531 (1999).
20. L. Li, J. Chandezon, G. Granet, and J. P. Plumey, "Rigorous and efficient grating-analysis method made easy for optical engineers," Appl. Opt. **38**, 304–313 (1999).
21. M. E. Inchaussandague and R. A. Depine, "Polarization conversion from diffraction gratings made of uniaxial crystals," Phys. Rev. E **54**, 2899–2911 (1996).
22. M. E. Inchaussandague and R. A. Depine, "Rigorous vector theory for diffraction gratings made of biaxial crystals," J. Mod. Opt. **44**, 1–27 (1997).
23. A. E. Dolinko and D. C. Skigin, "Enhanced method for determining the optical response of highly complex biological photonic structures," J. Opt. Soc. Am. A **30**, 1746–1759 (2013).
24. Y. Nakano, Y. Urade, R. Urade, and S. Kitaoka, "Isolation, purification, and characterization of the pellicle of euglena gracilis z.," J. Biochem. **102**, 1053–1063 (1987).
25. R. Drezek, A. Dunn, and R. Richards-Kortum, "Light scattering from cells: finite-difference time-domain simulations and goniometric measurements," Appl. Opt. **38**, 3651–3661 (1999).
26. A. Quirantes and S. Bernard, "Light-scattering methods for modelling algal particles as a collection of coated and/or nonspherical scatterers," J. Quantum Spectrosc. Radiat. Transfer **100**, 315–324 (2006).
27. O. Svensen, O. Frette, and S. Rune Erga, "Scattering properties of microalgae: the effect of cell size and cell wall," Appl. Opt. **46**, 5762–5769 (2007).
28. J. Dauchet, S. Blanco, J.-F. Cornet, and R. Fournier, "Calculation of the radiative properties of photosynthetic microorganisms," J. Quantum Spectrosc. Radiat. Transfer **161**, 60–84 (2015).
29. R. Kandilian, J. Pruvost, A. Artu, C. Lemasson, J. Legrand, and L. Pilon, "Comparison of experimentally and theoretically determined radiation characteristics of photosynthetic microorganisms," J. Quantum Spectrosc. Radiat. Transfer **175**, 30–45 (2016).
30. A. E. Dolinko, "From Newton's second law to Huygens's principle: visualizing waves in a large array of masses joined by springs," Eur. J. Phys. **30**, 1217–1228 (2009).
31. G. M. Hale and M. R. Querry, "Optical constants of water in the 200-nm to 200-μm wavelength region," Appl. Opt. **12**, 555–563 (1973).
32. U. Fano, "Effects of configuration interaction on intensities and phase shifts," Phys. Rev. **124**, 1866–1878 (1961).
33. A. E. Miroshnichenko, S. Flach, and Y. S. Kivshar, "Fano resonances in nanoscale structures," Rev. Mod. Phys. **82**, 2257–2298 (2010).
34. A. Hessel and A. A. Oliner, "A new theory of Wood's anomalies on optical gratings," Appl. Opt. **4**, 1275–1297 (1965).
35. A. Saito, "Material design and structural color inspired by biomimetic approach," Sci. Technol. Adv. Mater. **12**, 064709 (2011).
36. A. Riva and I. Algaba, "Ultraviolet protection provided by woven fabrics made with cellulose fibres: study of the influence of fibre type and structural characteristics of the fabric," J. Text. Inst. **97**, 349–358 (2006).